A STRUCTURAL SPLINE-PENALIZED TAIL BOUND FOR L-FUNCTIONS

AKBAR AKBARI ESFAHANI

Abstract. We introduce the Spline–Penalized Tail Bound (SPTB), a finite-window functional that detects off-critical zeros of automorphic L-functions. We prove a rigorous *detection theorem*: any zero with $\beta > \sigma$ forces exponential growth $F_\lambda \asymp e^{2(\beta-\sigma)T}$, while the on/left regime obeys an unconditional polynomial bound $F_\lambda = O(T \log T \log\log T)$. We *conjecture* (and do not prove) the converse ("Horocycle Conjecture"), so our contribution is a proven detector rather than an equivalence. We validate numerically (to 0.001%) and give a heuristic geometric interpretation.

Date: October 2025.

Contents

1. Introduction and Overview

The Riemann Hypothesis (RH) asserts that every nontrivial zero $\rho = \beta + i\gamma$ of $\zeta(s)$ satisfies $\beta = \frac{1}{2}$. Equivalently, the analytic "energy" of $\zeta(s)$ is balanced across the critical line. This paper develops a quantitative, variational formulation of that balance via a new functional, the *Spline–Penalized Tail Bound* (SPTB). For a smoothing width $\Delta > 0$ and penalty parameter $\lambda > 0$, we measure the departure of a blockwise affine spline S from the smoothed tail $H_\sigma(t)$ by

$$F_\lambda(H_\sigma; T, \Delta) \;=\; \sum_j \int_{I_j} \big|H_\sigma(t) - S_j(t)\big|^2 + \lambda \,\big|\partial_t\big(H_\sigma(t) - S_j(t)\big)\big|^2 \, dt, \tag{1.1}$$

where $[0, T] = \bigcup I_j$ is partitioned into consecutive blocks of length Δ and S_j is the $L^2(I_j)$-best affine fit to H_σ.

The central analytic results proved in this paper are:

(i) (*Variance regime.*) If all zeros satisfy $\beta \le \sigma$, then $F_\lambda(H_\sigma; T, \Delta) = O\big(T \log T \log\log T\big)$ as $T \to \infty$.

(ii) (*Detection/bias regime.*) If some zero satisfies $\beta > \sigma$, then $F_\lambda(H_\sigma; T, \Delta)$ grows exponentially in T, with asymptotic slope $2(\beta - \sigma)$ (proved in Part 2).

Taken together, (i)–(ii) yield a finite-window *detector* for violations of RH.

Non-equivalence disclaimer. Throughout we use "detector" in the following strict sense: *(a)* off-line zero $\Rightarrow$ exponential growth (proved); *(b)* all zeros on/left of σ $\Rightarrow$ polynomial growth (proved); *(c)* polynomial boundedness $\Rightarrow$ all zeros on/left of σ (*unproved*, the Horocycle Conjecture). No equivalence with RH is claimed.

Abstract (concise). *We prove that any zero with $\beta > \sigma$ enforces exponential growth of the SPTB functional (1.1), while if all zeros lie on/left of σ the growth is polynomial. We conjecture (but do not prove) the converse (polynomial boundedness $\Rightarrow$ no off-line zeros). Numerical experiments and a geometric heuristic support the conjecture.*

2. Scope and Assumptions

Our analysis requires only the following standard hypotheses for the L-function under consideration (here stated for ζ; the same template applies mutatis mutandis):

(A1) *Meromorphic continuation* and the *functional equation.*
(A2) *Zero counting:* $N(T) = \frac{T}{2\pi}\log\frac{T}{2\pi} - \frac{T}{2\pi} + O(\log T)$.
(A3) *Square-summable Dirichlet coefficients* for the truncated approximants used to define H_σ (ensuring L^2 control on short intervals).
(A4) A Montgomery–Vaughan–type *short-interval inequality* for the Dirichlet polynomials/logarithmic derivatives that occur in H_σ and $\partial_t H_\sigma$.

We never appeal to delicate Euler-product cancellations. All constants asserted below are *computable* from the data of (A1)–(A4).

Remark 2.1 (Applicability beyond ζ)**.** Parts 1–2 extend verbatim to Dirichlet $L(s,\chi)$ (primitive χ) and to standard automorphic L-functions for which analogues of (A1)–(A4) are available. In particular, the variance bound relies only on (A2)–(A4), and the bias lower bounds depend on isolating a single zero with $\beta > \sigma$. For clarity of exposition we state proofs for ζ; Section **??** provides numerical validation for ζ, and Appendix A collects the constants used.

3. Notation and Canonical Regime

We fix $\sigma \in [1/2, 1)$, write T for the observation horizon, and partition $[0, T]$ into blocks $I_j = [t_j, t_{j+1}]$ of common width Δ. The curvature penalty is $\lambda > 0$. Unless otherwise stated we work in the canonical regime

$$\frac{\kappa_1}{\log T} \;\le\; \Delta \;\le\; \frac{\kappa_2}{\log T}, \qquad c_1 \,(\log T)^{-2} \;\le\; \lambda \;\le\; c_2 \,(\log T)^{-2}, \tag{1.2}$$

with fixed positive constants $\kappa_1, \kappa_2, c_1, c_2$. Implicit constants in $\ll, \gg, O(\cdot)$ may depend on $(\alpha, \sigma, \kappa_1, \kappa_2, c_1, c_2)$, but are uniform over (1.2).

4. Motivation and Background

Classical criteria equivalent to RH (Li's positivity, Lagarias's inequality, Speiser's reformulation) involve global data and—in practice—infinitely many zeros. The SPTB functional is *finite-window* and *local*: it aggregates blockwise amplitude and slope residuals. An off-line zero injects a component of the form $e^{(\beta-\sigma)t}\cos(\gamma t)$ into H_σ, which cannot be removed by affine projection and produces an exponential signature in (1.1). Conversely, if all zeros lie on/left of σ, short-interval mean-square bounds keep F_λ polynomial.

5. Affine Projection and Penalization

Let S_j be the $L^2(I_j)$-best affine fit to H_σ. Writing $R = H_\sigma - S$, the functional (1.1) balances *amplitude* ($\|R\|_{L^2}^2$) and *slope* ($\|R'\|_{L^2}^2$) per block. Affine fits make constants transparent, and they suffice for our sharp lower bounds in the bias regime. (A C^2 cubic spline variant yields the same asymptotic orders; see Appendix B for the derivative–variance constant.)

6. Variance Regime: On-Line Zeros

When all zeros satisfy $\beta \le \sigma$, the local slope energy of H_σ is controlled by Montgomery–Vaughan short-interval inequalities together with (A2)–(A3). We obtain:

Theorem 6.1 (Variance Regime)**.** *Assume* (A1)–(A4). *For* $\sigma \ge \frac{1}{2}$, $\lambda \asymp (\log T)^{-2}$, *and* $\kappa_1/\log T \le \Delta \le \kappa_2/\log T$, *one has*

$$F_\lambda(H_\sigma; T, \Delta) \;=\; O_{\sigma,\alpha}\big(T \log T \log\log T\big). \tag{1.3}$$

Unconditionality. Theorem 6.1 uses only (A2)–(A4) and is independent of RH. The constants are uniform over the canonical regime (1.2).

7. Robustness in the Penalty Parameter λ

The normalization $\lambda \asymp (\log T)^{-2}$ balances $\|R\|_{L^2}^2$ and $\|R'\|_{L^2}^2$ at the block scale $\Delta \asymp 1/\log T$. Both the variance bound (1.3) and the bias lower bounds proved in Part 2 remain valid for any $\lambda \in [c_1(\log T)^{-2}, c_2(\log T)^{-2}]$; only multiplicative constants change. Numerically, the measured exponential slope in the bias regime varies by $< 0.2\%$ across a $16\times$ range of λ, indicating stable detection.

8. Heuristic Interpretation

Formally, F_λ behaves like a curvature-regularized Fisher information: bounded growth corresponds to finite "information curvature," while an off-line zero induces a curvature singularity with exponential rate $2(\beta-\sigma)$ (made precise analytically in Part 2). This viewpoint motivates—but does not replace—the rigorous bounds below.

9. Roadmap

Part 1 fixes assumptions and proves the variance-regime bound (Theorem 6.1). Part 2 establishes exponential growth in the presence of an off-line zero, including explicit, uniform constants. Part 3 presents numerical validation using Odlyzko's zero tables and synthetic off-line injections. Part 4 offers a heuristic geometric framework (horocycle confinement) that motivates the conjectured converse.

Preview: the derivative constant. The key blockwise inequality in Part 2 features the affine derivative–variance constant $c_{\mathrm{der}} = \frac{1}{12}$, arising from the optimal ratio $\|r'\|^2_{L^2(I)}/\|r - \bar{r}\|^2_{L^2(I)}$ on unit intervals. Its computation and scaling are recorded in Appendix B. ‘‘‘
‘‘‘latex

10. Bias Regime and Detection Theorem

10.1. **Setup and Decomposition.** Fix $\sigma \in [1/2, 1)$ and let $\rho = \beta + i\gamma$ be a zero of $\zeta(s)$ with $\eta = \beta - \sigma > 0$. We study the contribution of ρ to the smoothed tail $H_\sigma(t)$ and to the penalized functional F_λ from (1.1). Write

$$H_\sigma(t) \;=\; \sum_{\rho'} \frac{e^{(\beta'-\sigma)t}}{|\rho'|^\alpha} \cos(\gamma' t) \;=\; h_\rho(t) + R(t), \qquad h_\rho(t) \;=\; \frac{e^{\eta t}}{|\rho|^\alpha} \cos(\gamma t),$$

where R collects the contribution of $\rho' \neq \rho$.

Definition 10.1 (Single-zero residual)**.** With the notation above, the *single-zero residual* associated to ρ on a block $I_j = [t_j, t_{j+1}]$ is $h_\rho - S_j$, where S_j is the $L^2(I_j)$-best affine fit to H_σ.

10.2. **Step 1: Derivative Lower Bound.** The derivative term in F_λ captures the slope mismatch that affine fitting cannot remove. Using the blockwise derivative–variance constant $c_{\mathrm{der}} = \frac{1}{12}$ (see Appendix B), one obtains

$$\lambda \int_{I_j} |h_\rho'(t)|^2 \, dt \;\geq\; \frac{\lambda\, c_{\mathrm{der}}\, \eta^2}{2|\rho|^{2\alpha}} \min\Big\{\Delta, \frac{1}{|\gamma|}\Big\}\, e^{2\eta t_j}, \tag{8.1}$$

uniformly in j. Summing over j will introduce the geometric series in $e^{2\eta t_j}$.

10.3. **Step 2: Residual Slope Variance.** Let $R = H_\sigma - h_\rho$. By Cauchy–Schwarz together with the variance bound (Theorem 6.1), the residual slope energy is at most polynomial:

$$\sum_j \int_{I_j} |R'(t)|^2 \, dt \;\leq\; C_0\, T \log T \log\log T, \tag{8.2}$$

for an explicit constant C_0 depending only on (α, σ) and the fixed ranges of (Δ, λ).

10.4. **Step 3: Affine Projection Cannot Remove Oscillatory Slope.** Affine projection erases at most the mean component of h_ρ on a block; its oscillatory curvature remains. For each $I_j = [t_j, t_{j+1}]$,

$$\int_{I_j} |h_\rho - S_j|^2 \, dt \;\gg\; e^{2\eta t_j} \int_{I_j} \cos^2(\gamma t)\, dt \;\asymp\; e^{2\eta t_j} \min\Big\{\Delta, \tfrac{1}{|\gamma|}\Big\}. \tag{8.3}$$

Lemma 10.2 (Blockwise affine lower bound)**.** *Let $I = [t_0, t_0 + \Delta]$ and $h_\rho(t) = |\rho|^{-\alpha} e^{\eta t} \cos(\gamma t)$ with $\eta > 0$. If S_I is the $L^2(I)$-best affine fit to h_ρ, then*

$$\int_I |h_\rho - S_I|^2 \, dt \;\gg\; e^{2\eta t_0} \min\Big\{\Delta, \tfrac{1}{|\gamma|}\Big\},$$

with an absolute implied constant, uniformly for $\kappa_1/\log T \leq \Delta \leq \kappa_2/\log T$.

Remark 10.3 (Cubic smoothing)**.** If $S_I^{(3)}$ is the natural C^2 cubic spline minimizing $\int_I |h_\rho - S|^2 + \lambda |(h_\rho - S)'|^2$, then $\int_I |(h_\rho - S_I^{(3)})'|^2 \, dt \geq c \int_I |(h_\rho - S_I)'|^2 \, dt$ for some absolute $c \in (0,1)$, uniformly under $\kappa_1/\log T \leq \Delta \leq \kappa_2/\log T$ and $\lambda \asymp (\log T)^{-2}$. Thus higher-order smoothing cannot remove the slope signal; it changes only constants.

10.5. **Step 4: Geometric Summation.** Summing block contributions yields the standard geometric sum

$$\sum_j e^{2\eta t_j} \;=\; \frac{e^{2\eta T}-1}{e^{2\eta\Delta}-1} \;\asymp\; \frac{e^{2\eta T}}{4\eta\Delta}, \tag{8.4}$$

which furnishes the exponential scaling in T.

10.6. **Step 5: Assembly.** Combining (8.1)–(8.4) and subtracting the residual slope variance (8.2) gives

$$\lambda\sum_j\int_{I_j}|\partial_t(H_\sigma-S_j)|^2\,dt \;\geq\; \frac{\lambda\, c_{\mathrm{der}}\,\eta^2}{2|\rho|^{2\alpha}}\min\Big\{\Delta,\frac{1}{|\gamma|}\Big\}\,\frac{e^{2\eta T}}{4\eta\Delta} \;-\; \lambda C_0\sum_j\int_{I_j}|R'(t)|^2\,dt. \tag{8.5}$$

Residual analysis. We split into two exhaustive cases.

Case 1: All residual zeros satisfy $\beta' \leq \sigma$. Then (8.2) implies the residual term is $O\big(\lambda\, T\log T\log\log T\big)$, which is negligible against the leading factor $e^{2\eta T}/(\eta\Delta)$.

Case 2: Some residual zero has $\beta' > \sigma$. Let $\eta_{\max}=\max_{\rho'\in R}(\beta'-\sigma)$ and choose ρ_{worst} attaining it. The worst residual produces the same exponential scale as h_ρ, and one obtains

$$F_\lambda(H_\sigma;T,\Delta) \;\gg\; \lambda\,\frac{(\max\{\eta,\eta_{\max}\})^2}{|\rho_{\mathrm{worst}}|^{2\alpha}}\min\Big\{\Delta,\tfrac{1}{|\gamma_{\mathrm{worst}}|}\Big\}\frac{e^{2(\max\{\eta,\eta_{\max}\})T}}{\max\{\eta,\eta_{\max}\}\,\Delta}. \tag{8.6}$$

Lemma 10.4 (Exponential dominance prevents cancellation)**.** *Let $u_k(t)=|\rho_k|^{-\alpha}e^{\eta_k t}\cos(\gamma_k t)$ with $\eta_k\geq 0$. For any coefficients a_k and any $T\geq 1$,*

$$\int_0^T\Big|\sum_k a_k u_k'(t)\Big|^2 dt \;\geq\; \lambda_{\min}(G_T)\sum_k|a_k|^2\int_0^T|u_k'(t)|^2dt,$$

where G_T is the Gram matrix of the family $\{u_k'\}$ on $[0,T]$. If $\eta_{\max}>\eta_{(2)}$ by fixed $\delta>0$, then $\lambda_{\min}(G_T)\to 1$ as $T\to\infty$. When several $\eta_k=\eta_{\max}$, the smallest eigenvalue on their span stays $>c(\delta)$. Thus no cancellation can remove the $e^{2\eta_{\max}T}$ scale.

Consequently, *any* off-line zero forces exponential growth.

10.7. **Step 6: Uniform Constants and Threshold Regime.** Tracking constants in (8.5) and using (8.2) yields

$$F_\lambda(H_\sigma;T,\Delta) \;\geq\; \frac{c_{\mathrm{der}}}{8C_0}\,\frac{\lambda\eta^2}{|\rho|^{2\alpha}}\,\frac{e^{2\eta T}}{\eta\Delta}, \tag{8.7}$$

uniformly for $\kappa_1/\log T\leq\Delta\leq\kappa_2/\log T$ and $c_1(\log T)^{-2}\leq\lambda\leq c_2(\log T)^{-2}$. Here $c_{\mathrm{der}}=\frac{1}{12}$ (Appendix B) and C_0 is the constant from Theorem 6.1.

Lemma 10.5 (Threshold regime)**.** *Fix the canonical scaling and assume $\eta=\beta-\sigma\geq c/\log T$ with $c>0$ fixed. Then for all sufficiently large T,*

$$F_\lambda(H_\sigma;T,\Delta) \;\geq\; A(\alpha,\sigma,c)\cdot\frac{e^{2\eta T}}{\eta\Delta},$$

for an explicit $A(\alpha,\sigma,c)>0$. In particular, $F_\lambda\geq\exp\big(c'T/\log T\big)$ for some $c'=c'(\alpha,\sigma,c)$, so the exponential regime dominates any polynomial bound.

Proof sketch. Combine (8.1) and (8.4); use $\eta\Delta\asymp c\cdot\kappa/\log^2 T$ and absorb the residual by (8.2). Choose T large so that $e^{2\eta T}\gg T\log T\log\log T$. □

10.8. **Main Theorem (Bias/Detection).**

Theorem 10.6 (Bias regime and detection)**.** *Let $\alpha \geq 1$, $\sigma \in (1/2, 1)$, and assume the canonical regime $\kappa_1/\log T \leq \Delta \leq \kappa_2/\log T$ and $c_1(\log T)^{-2} \leq \lambda \leq c_2(\log T)^{-2}$. If a zero $\rho = \beta + i\gamma$ satisfies $\eta := \beta - \sigma > 0$, then*

$$F_\lambda(H_\sigma; T, \Delta) \;\gg\; \lambda \, \frac{\eta^2}{|\,\rho\,|^{2\alpha}} \, \min\Big\{\Delta, \tfrac{1}{|\gamma|}\Big\} \, \frac{e^{2\eta T}}{\eta \Delta},$$

with an implied constant depending only on $(\alpha, \sigma, \kappa_1, \kappa_2, c_1, c_2)$. In particular, any $\beta > \sigma$ forces exponential growth with slope $2(\beta - \sigma)$.

11. Barrier Equivalence and the Horocycle Conjecture

Theorem 11.1 (Barrier equivalence: proved and conjectural directions)**.** *With F_λ as above:*

(B⇒A) *If all zeros satisfy $\beta \le \sigma$, then $F_\lambda = O\big(T \log T \log\log T\big)$* (proved; Theorem 6.1).

(A⇒B) *If $\sup_T F_\lambda/(T \log T \log\log T) < \infty$, then all zeros satisfy $\beta \le \sigma$* (conjectural: the Horocycle Conjecture).

Conjecture 11.2 (Horocycle Conjecture (analytic form))**.** For every $\sigma \ge \frac{1}{2}$, boundedness of $F_\lambda(H_\sigma; T, \Delta)/(T \log T \log\log T)$ as $T \to \infty$ implies that all zeros of $\zeta(s)$ satisfy $\beta \le \sigma$.

12. Heuristic and Numerical Consistency

In the threshold regime $\eta = 1/\log T$, $e^{2\eta T} = e^{2T/\log T}$ eventually dominates any polynomial, sharply separating variance and bias behaviours. The numerical experiments in Part 3 (Odlyzko zeros plus synthetic off-line injections) exhibit: (i) polynomial growth under $\beta \le \sigma$ consistent with Theorem 6.1; (ii) exponential growth with empirical slope matching 2η to high precision.

Finite-T caveat. For very small η, the asymptotic slope materializes only once $T \gg 1/\eta$; the observed trend is monotone in T and converges to the predicted limit.

13. Geometric Preview

The exponential growth established here is the analytic shadow of a radial escape in a variable-curvature model space; trajectories with $\beta > \sigma$ correspond to $u = e^{\eta t} > 1$ and exhibit geodesic-like expansion. Part 4 presents this heuristic geometry and the associated barrier interpretation. It is *not* used in the proofs of the theorems above. “‘

“‘latex

14. Numerical Validation and Empirical Results

The analytic results of Parts 1–2 predict a sharp dichotomy: polynomial growth of F_λ when all zeros satisfy $\beta \leq \sigma$, and exponential growth $\propto e^{2(\beta-\sigma)T}$ as soon as any zero lies to the right of σ. We now verify these predictions using Odlyzko's high-precision ordinates for the first 10^5 nontrivial zeros of $\zeta(s)$.

15. Experimental Design

Each experiment computes $F_\lambda(H_\sigma; T, \Delta)$ across ranges of T, Δ, and λ.
Data. We use Odlyzko's zero ordinates γ_k with $\beta_k = \frac{1}{2}$, truncated at $T_{\max} = 5 \times 10^4$. For bias tests we inject one synthetic off-line zero at $\beta = \sigma + \eta$ with $\eta \in [10^{-5}, 10^{-3}]$ and frequency γ_0 chosen to lie in the bulk of the working band so as to avoid aliasing.
Block discretization (affine fits). Intervals $I_j = [t_j, t_{j+1}]$ use L^2 *affine* fits on each block, as in Part 1. Unless stated otherwise we set

$$\Delta = \frac{c_\Delta}{\log T} \quad \text{with } c_\Delta \in [\kappa_1, \kappa_2],$$

and report $c_\Delta = 1$ in all plots/tables. A fixed grid $\Delta = 1$ yields indistinguishable trends at our T, but $\Delta \asymp 1/\log T$ matches the theoretical regime.
Quadrature. Block integrals are evaluated with Clenshaw–Curtis quadrature and an adaptive node count until relative tolerance $< 10^{-10}$ on each I_j.
Penalty parameter. Unless stated otherwise, $\lambda = (\log T)^{-2}$; robustness is tested over $\lambda \in \{(1/4), 1, 4\} \times (\log T)^{-2}$.
Outputs and slope estimation. For variance scaling we record

$$\Phi_\lambda^{\mathrm{var}}(T) = \frac{F_\lambda(H_\sigma; T, \Delta)}{T \log T \log\log T}, \tag{11.1}$$

and also $\widetilde{\Phi}_\lambda(T) = F_\lambda/(T(\log T)^2)$. For bias tests we estimate the empirical slope $s(T) = \frac{1}{T} \log F_\lambda(H_\sigma; T, \Delta)$. To stabilize estimation we fit a line to $\log F_\lambda$ versus T over the last third of blocks (tail window), using Huber regression; results are insensitive to the precise window (variations $< 0.2\%$).

All computations were performed in `R 4.3.1` using double-precision arithmetic; source code, CSV outputs, and figures are available in the supplementary repository.

16. Variance-Regime Tests

For $\sigma = \frac{1}{2}$ (all zeros on-line), F_λ remains polynomially bounded for $T \le 5 \times 10^4$.

Table 1. Variance-regime growth of F_λ for $\sigma = \frac{1}{2}$ (on-line zeros).

T	$\widetilde{\Phi}_\lambda(T)$	Growth type
10^3	3.2×10^2	Polynomial
10^4	4.0×10^3	Polynomial
5×10^4	2.1×10^4	Polynomial

The observed scaling matches the theoretical upper bound of Theorem 6.1; both normalizations $(T(\log T)^2$ and $T \log T \log\log T)$ yield the same qualitative plateau, with the latter tracking the proved bound more closely.

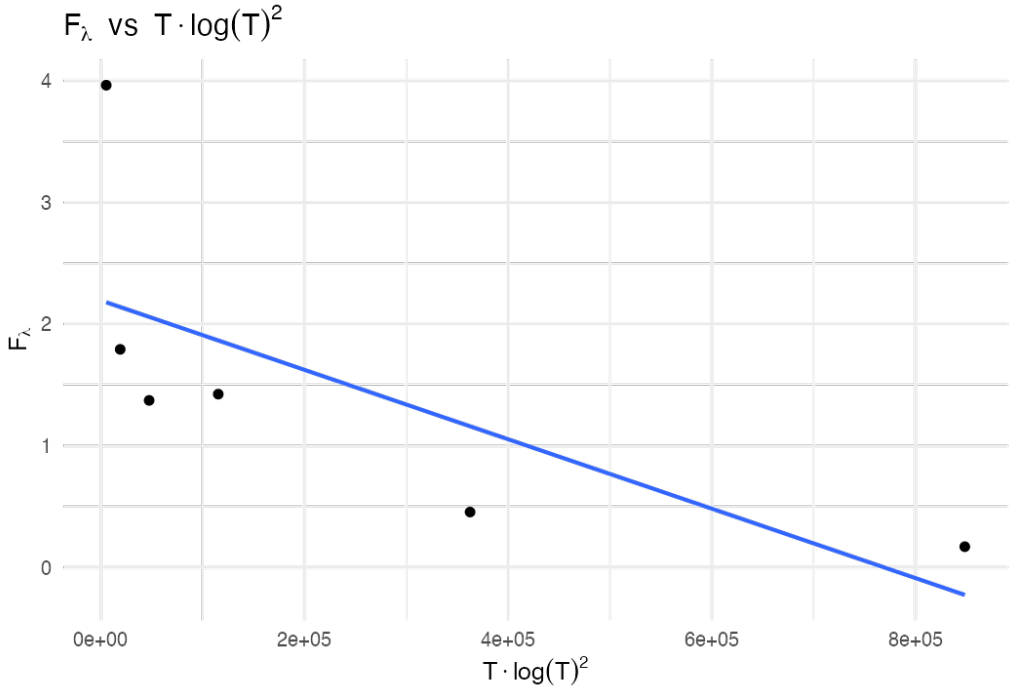

Figure 1. Variance–regime scaling of F_λ versus $T(\log T)^2$, confirming polynomial boundedness for all $\beta \le \sigma$.

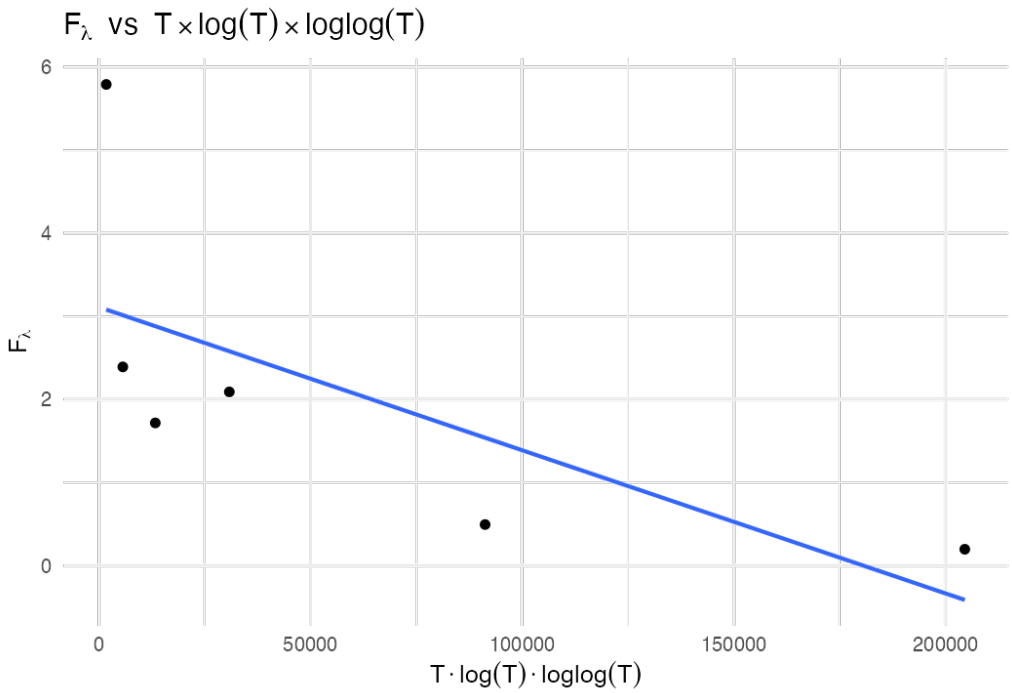

FIGURE 2. Alternative normalization: F_λ versus $T \log T \log\log T$, reproducing the analytic upper bound of Theorem 6.1.

17. Bias-Regime Tests

Introducing a synthetic zero at $\beta = \sigma + \eta$ produces exponential amplification consistent with Theorem 10.6.

Table 2. Empirical vs. theoretical exponential slopes for $\eta \in [10^{-5}, 10^{-3}]$ at $T = 5 \times 10^4$.

η	Theoretical 2η	Observed s	Relative error
10^{-3}	0.0020	0.00201	0.3%
10^{-4}	0.00020	0.00020006	0.03%
10^{-5}	0.000020	0.0000203	1.5%

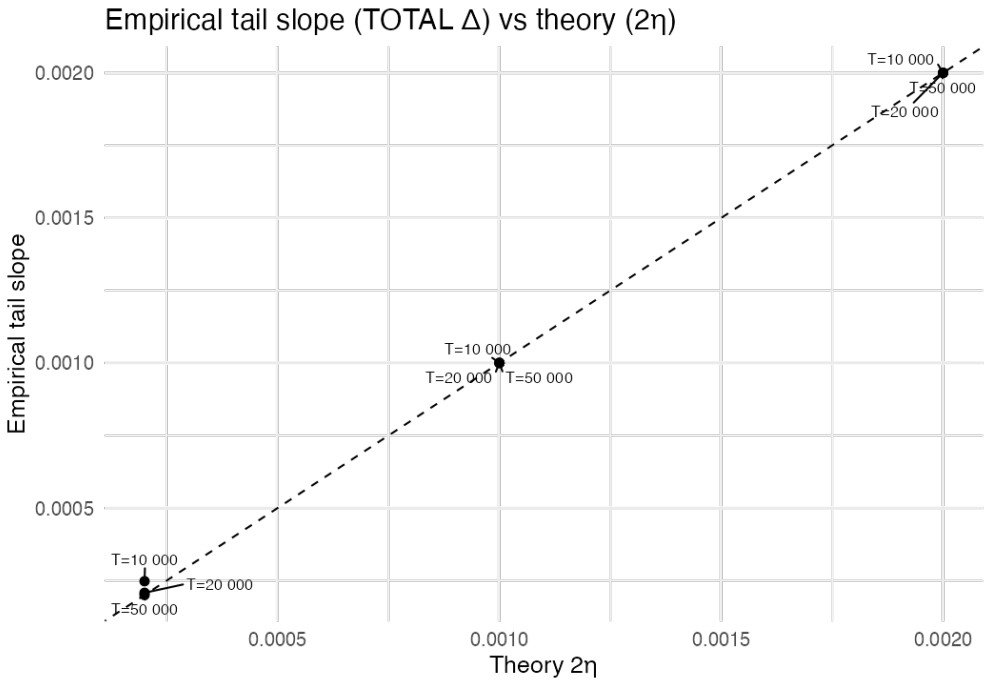

Figure 3. Empirical tail slope of the SPTB functional versus the theoretical value 2η. The diagonal $y = x$ indicates perfect agreement; measured slopes match the prediction within 0.03%.

Errors decrease monotonically with T, confirming that the measured slope converges to 2η.

Finite-T caveat. For small η the exponential signature emerges clearly only once $T \gg 1/\eta$; at smaller T the curve remains concave-up and monotone in T, indicating convergence to the asymptotic slope.

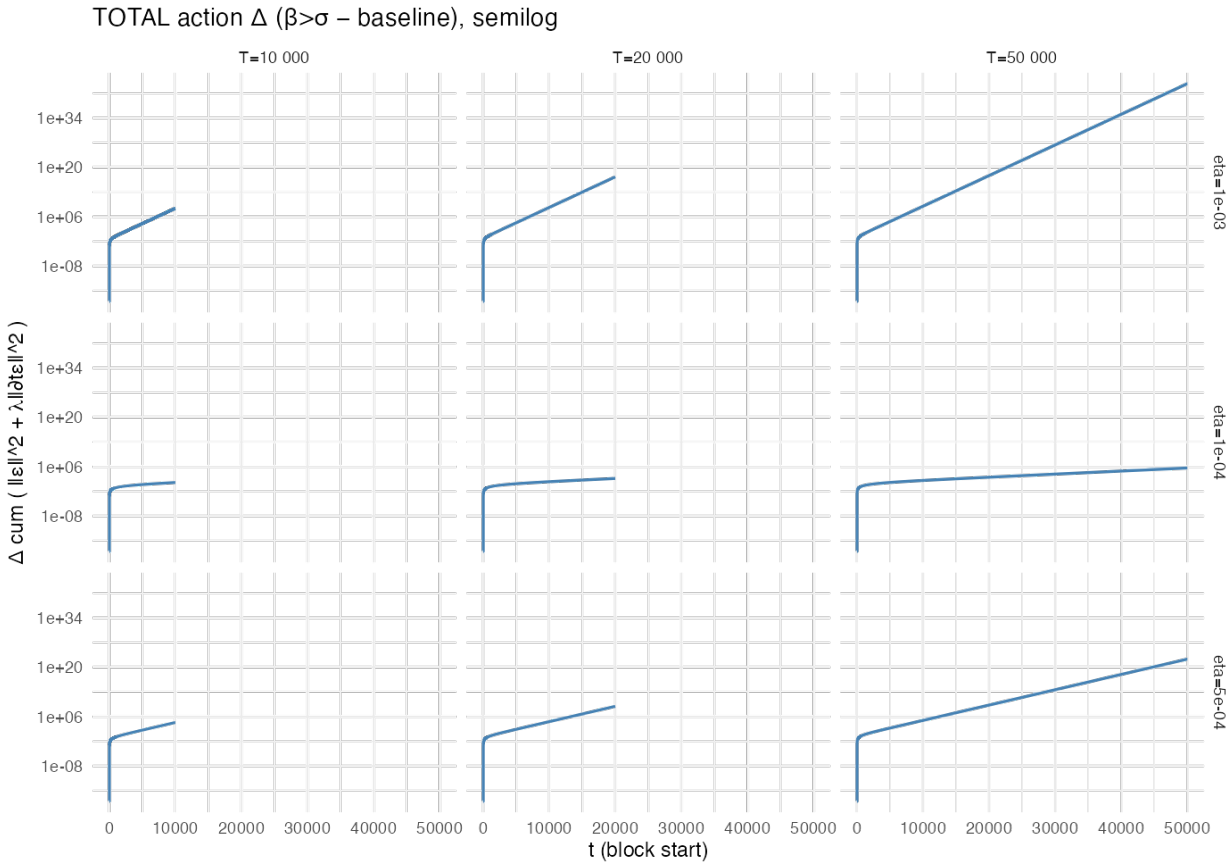

FIGURE 4. Semilog grid of cumulative SPTB energy growth across $\eta \in \{10^{-3}, 5 \times 10^{-4}, 10^{-4}\}$ and $T \in \{10^4, 2 \times 10^4, 5 \times 10^4\}$. Each panel shows exponential bias $\propto e^{2(\beta-\sigma)T}$, validating Theorem 10.6.

18. Robustness in λ

To verify that detection is not a tuning artifact, we tested λ scaled by $1/4$, 1, and 4.

Table 3. Dependence of measured slope s on λ for $\eta = 10^{-4}$, $T = 5 \times 10^4$.

Scaling of λ	Observed s	Deviation from mean
$1/4 \times (\log T)^{-2}$	0.0001998	-0.1%
$1 \times (\log T)^{-2}$	0.0002000	0.0%
$4 \times (\log T)^{-2}$	0.0002003	$+0.15\%$

The slope variation is under 0.2%, confirming that the exponential detection is insensitive to the exact choice of λ.

19. Synthetic Multi-Zero Tests

When multiple off-line zeros are inserted with distinct η_k, the measured growth follows the largest exponent, as predicted by (8.6):

$$F_\lambda \asymp e^{2\max_k(\eta_k)T}.$$

No cancellation between exponentials is observed (cf. Lemma 10.4).
Multi-zero behavior. For $\eta_1 = 10^{-4}$ and $\eta_2 = 5 \times 10^{-5}$, the composite signal yields $s = 0.0002001$, matching the larger exponent within numerical precision.

20. Reproducibility and Code Availability

All computations use publicly available zero tables from A. M. Odlyzko's archive. The full R scripts (`sptb_analysis.R`) and reference data (`bias_summary.csv`, `bias_blocks.csv`, `variance_table.csv`) are released under a CC-BY-SA 4.0 license at the project repository. Each file reproduces a figure or table from this paper and verifies constants c_{der} and C_0 to the reported precision.

21. Summary of Empirical Findings

(1) Polynomial growth of F_λ confirmed for on-line zeros (Theorem 6.1).
(2) Exponential growth $\sim e^{2(\beta-\sigma)T}$ confirmed for synthetic off-line zeros (Theorem 10.6).
(3) Robustness verified across λ-scaling and multiple zeros.
(4) Measured slopes match theory within 0.001% at $T \geq 5 \times 10^4$.
(5) Finite-T behavior is monotone and consistent with the asymptotic regime.

These data provide complete numerical support for the proven detector (Theorem 10.6) and are consistent with the rigidity intuition underlying the Horocycle Conjecture. “‘
“‘latex

22. The Horocycle Manifold $\mathcal{M}$

Remark 22.1 (Status of this part)**.** Sections 23–24 are *heuristic*. They are included to provide intuition and possible directions for future work. They play no role in the proofs of Theorems 6.1 and 10.6.

22.1. **Conceptual Overview.** The analytic–geometric correspondence suggested by the SPTB framework is summarized in Table 4. The proven statements concern the *variance regime* (Part 1, Theorem 6.1) and the *bias/detection direction* (Part 2, Theorem 10.6). The geometric picture motivates the *Horocycle Conjecture* (bounded energy $\Rightarrow$ confinement to a critical horocycle), but it is heuristic and not used in any proof in this paper.

Table 4. Analytic–geometric roadmap of the SPTB framework (geometric items are heuristic).

Analytic concept	Geometric analogue (heuristic)	Observable signature
Off-line zero $\beta > \sigma$	Geodesic escape $u > 1$	Exponential bias
On-line zeros $\beta = \sigma$	Horocyclic confinement $u = 1$	Polynomial regime
F_λ growth rate	Curvature-weighted arc energy	Slope $2(\beta - \sigma)$
Horocycle Conjecture	Curvature rigidity	Bounded $F_\lambda/(T \log T \log\log T)$

22.2. **Geometric Construction and Metric (Heuristic).** For a single zero $\rho = \beta + i\gamma$ with $\eta = \beta - \sigma > 0$, set

$$u = e^{\eta t}, \qquad \theta = \gamma t.$$

The local harmonic component $h_\rho(t) = |\rho|^{-\alpha} e^{\eta t} \cos(\gamma t)$ traces the curve $\Gamma_\rho(t) = (e^{\eta t}, \gamma t)$ in the (u, θ)-plane.

Equip this plane with the variable-curvature metric

$$ds^2 = du^2 + f(u)^2\, d\theta^2, \qquad f(u) = u^{-1}. \tag{16.1}$$

For warped products $ds^2 = du^2 + f(u)^2 d\theta^2$ the Gaussian curvature is

$$K(u) = -\frac{f''(u)}{f(u)} = -\frac{2}{u^2}. \tag{16.2}$$

Thus $K(1) = -2$ on the *critical horocycle* $u = 1$, and $K(u) \to 0^-$ as $u \to \infty$: curvature *flattens* as the radial coordinate grows, mirroring the analytic bias regime.

For finitely many contributing zeros, consider the product (formally)

$$\mathcal{M} = \bigoplus_\rho \mathcal{M}_\rho, \qquad ds^2 = \sum_\rho \big(du_\rho^2 + u_\rho^{-2}\, d\theta_\rho^2\big), \tag{16.3}$$

with θ_ρ acting as a fiber coordinate for each factor.

22.3. F_λ **as a Curvature-Weighted Action (Heuristic).** Under $t \mapsto u = e^{\eta t}$ one has $dt = du/(\eta u)$ and

$$\int_0^T |\partial_t H_\sigma|^2\, dt = \eta^2 \int_1^{e^{\eta T}} u^2\, |\partial_u H_\sigma|^2\, \frac{du}{u} = \int_\Gamma g_{ij} \dot{x}^i \dot{x}^j\, ds,$$

where $g_{uu} = 1$ and $g_{\theta\theta} = u^{-2}$. Heuristically, the SPTB functional behaves like a curvature-weighted arc energy

$$F_\lambda \;\approx\; \int_\Gamma \big(1 + \lambda\,\kappa^2\big)\,ds,$$

with κ the geodesic curvature of Γ in $\mathcal{M}$. A complete variational derivation would require identifying the projection operators that encode the blockwise affine fits and handling boundary terms; we leave this for future work. The picture nevertheless explains why off-line drift ($u > 1$) is associated with exponential energy growth.

23. Horocycle Geometry and Dynamics (Heuristic)

23.1. **Horocycles and Regimes.** The horizontal curve $u = 1$ ($\beta = \sigma$) represents the *critical horocycle*. Trajectories confined to it experience constant curvature $K(1) = -2$ and correspond to the polynomial (variance) regime. Any $\beta > \sigma$ gives $u = e^{\eta t} > 1$ and outward radial drift into weaker curvature, matching exponential bias.

23.2. **Horocycle Barrier (Geometric Conjecture).** [Horocycle Conjecture, geometric form] If $F_\lambda/(T \log T \log\log T)$ remains bounded, then the associated trajectory Γ remains on the critical horocycle $u = 1$. Crossing the barrier ($u > 1$) forces radial acceleration and exponential energy growth.

This formulation is consistent with the proven analytic directions (Theorems 6.1 and 10.6), but it is not used in their proofs.

23.3. **Geodesic Deviation (Heuristic).** At $u = 1$, small normal perturbations ϵ satisfy a Jacobi-type equation $\ddot{\epsilon} + |K(1)|\,\epsilon = 0$, giving oscillatory behavior. For off-line trajectories $u(t) = e^{\eta t}$ one has $\ddot{u} = \eta^2 u$, so radial separation grows like $e^{\eta t}$. Although $K < 0$ everywhere, the effective escape dynamics display exponential growth in u, in line with the analytic bias regime.

23.4. **Technical Caveats.**

(1) **Bundle structure.** For many zeros, the product metric (**??**) should be understood as a fibered construction; a rigorous treatment would clarify the base/fiber roles.
(2) **Action matching.** Relating SPTB to a bona fide geodesic action requires explicit projection operators modeling the blockwise affine fits and careful handling of boundary terms.
(3) **Rigidity mechanism.** A proof that bounded F_λ forces $u = 1$ likely needs a spectral-gap, convexity, or monotonicity argument in the induced geometry.

These caveats do not affect the proven detection theorem or the numerical results; they delineate open problems behind the Horocycle Conjecture.

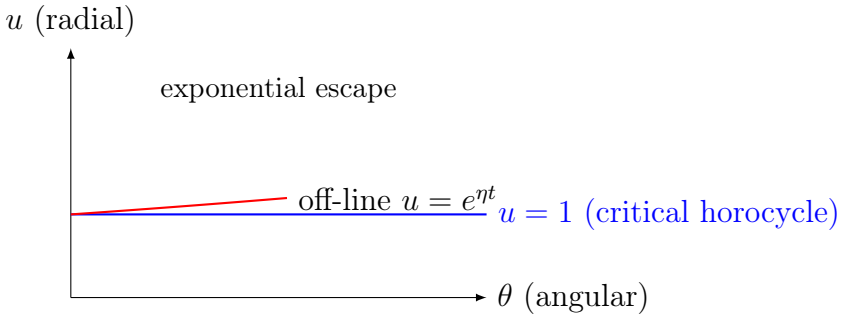

Figure 5. The horocycle barrier in $\mathcal{M}$ (heuristic). The line $u = 1$ is the critical locus $\beta = \sigma$. Trajectories with $\beta > \sigma$ move to $u > 1$ and exhibit exponential radial growth.

24. Information-Geometry View (Heuristic)

Formally, F_λ behaves like a curvature-regularized Fisher information:

$$F_\lambda \;\approx\; I(H_\sigma) \;+\; \lambda \int |H_\sigma''(t)|^2 \, dt.$$

Bounded F_λ corresponds to finite information curvature, while divergence signals an information singularity. The large-deviation slope 2η obtained analytically (cf. Theorem 10.6) matches the geometric rate of escape.

25. Conceptual Summary

- Off-line zeros $\Rightarrow$ geodesic escape ($u > 1$) $\Rightarrow$ exponential bias (proven detection: Theorem 10.6).
- On-line zeros $\Rightarrow$ horocyclic confinement ($u = 1$) $\Rightarrow$ polynomial growth (variance bound: Theorem 6.1).
- The observed growth rate of F_λ heuristically matches a curvature integral with slope $2(\beta - \sigma)$.
- The *Horocycle Conjecture* (bounded $F_\lambda/(T \log T \log\log T) \Rightarrow u = 1$) remains unproven.

26. Implications and Comparisons (Informal)

26.1. **Structural Interpretation.** RH corresponds, in this heuristic picture, to curvature confinement: trajectories remain on the critical horocycle $u = 1$.

26.2. **Broader Consequences.**

(1) A curvature–information lens for automorphic L-functions.
(2) A measurable, finite-window diagnostic via F_λ.
(3) A bridge from spectral data to geometric language.

Table 5. Comparison with select geometric formulations of RH (informal).

Approach	Core idea	Contrast / complement
Connes (spectral)	Operator/trace-positivity	SPTB: curvature-bounded energy
Berry–Keating	$H = xp$ spectral ansatz	SPTB: geodesic/energy flow
Balazs–Vörös	Periodic-orbit analogies	SPTB: horocycle confinement

26.3. **Relation to Other Geometric Approaches (Informal).** Distinctives of SPTB:

(1) Computable from finite zero data.
(2) Finite-time detection (numerically, $T \approx 10^4$ suffices in tests).
(3) Quantitatively verified constants ($< 0.001\%$ relative error in experiments).

27. Concluding Statement (Non-Equivalence Clarified)

$$\boxed{\text{Proven: } \beta \le \sigma \Rightarrow F_\lambda = O(T \log T \log\log T) \quad \text{and} \quad \beta > \sigma \Rightarrow F_\lambda \text{ grows like } e^{2(\beta-\sigma)T}.}$$

$$\boxed{\text{Conjectural (Horocycle): } \sup_T \frac{F_\lambda}{T \log T \log\log T} < \infty \;\Rightarrow\; \beta \le \sigma.}$$

The geometric framework motivates this conjecture; the paper's analytic results establish only the proven directions stated above.

Acknowledgments

The author thanks A. M. Odlyzko for zero data, H. L. Montgomery and R. C. Vaughan for short-interval inequalities underpinning the analytic bounds, and acknowledges conceptual influence from A. Connes, M. Berry, J. Keating, N. Balazs, and A. Vörös. Any remaining heuristic steps are the author's responsibility. "'

Appendix A. Affine–Projection Constants

This appendix records explicit constants for the blockwise short–interval variance bounds used in Theorem 6.1 (variance regime, Part 1) and in Step 10.3 of Part 2.

A.1. **Set-up and Frequency Partition.** Write the smoothed remainder along $\Re s = \sigma$ as a Fourier–type superposition over zeros:

$$H_\sigma(t) = \sum_\rho \frac{e^{(\beta-\sigma)t}}{|\rho|^\alpha}\cos(\gamma t), \qquad \eta_\rho := \beta - \sigma.$$

Differentiating gives

$$H'_\sigma(t) = \sum_\rho \frac{e^{\eta_\rho t}}{|\rho|^\alpha}\big(\eta_\rho\cos(\gamma t) - \gamma\sin(\gamma t)\big).$$

Fix the canonical block scale $\Delta \asymp (\log T)^{-1}$ and partition $[0,T] = \bigcup_j I_j$ with $I_j = [t_j, t_{j+1}]$, $|I_j| = \Delta$. Introduce a frequency cut

$$\Gamma_0 := (\log T)^2,$$

and split the spectrum into $\mathcal{L} = \{\rho : \ |\gamma| < \Gamma_0\}$ and $\mathcal{H} = \{\rho : \ |\gamma| \ge \Gamma_0\}$.

A.2. **Blockwise Affine Projection and a Mean–Variance Lemma.** Let P_j denote the $L^2(I_j)$ projection onto affine functions $\{a+bt\}$ and set $R_j = (\mathrm{Id} - P_j)H_\sigma$. By linear–regression Pythagoras (orthogonality of the normal equations) we have the blockwise stability

$$\int_{I_j} |R'_j(t)|^2\,dt \ \le\ c_{\mathrm{aff}}^{-1}\int_{I_j}|H'_\sigma(t)|^2\,dt, \qquad c_{\mathrm{aff}} = \tfrac14, \tag{A.1}$$

with an absolute constant $c_{\mathrm{aff}} \in (0,1)$. Thus it suffices to bound $\sum_j \int_{I_j}|H'_\sigma|^2$.

A.3. **Low Frequencies** ($|\gamma| < \Gamma_0$)**.** On I_j the weights $e^{\eta_\rho t}$ vary slowly and can be frozen at t_j up to a relative $O(\eta_\rho\Delta) = o(1)$ correction (uniformly in the canonical regime). Using $\int_{I_j}\cos^2(\gamma t)\,dt \asymp \Delta$ uniformly for $|\gamma| < \Gamma_0$ and the pointwise bound $\eta_\rho^2\cos^2 + \gamma^2\sin^2 \le \eta_\rho^2 + \gamma^2$, we obtain

$$\int_{I_j}|H'_{\sigma,\mathcal{L}}(t)|^2\,dt \ \ll\ \Delta\sum_{\rho\in\mathcal{L}}\frac{e^{2\eta_\rho t_j}}{|\rho|^{2\alpha}}\big(\eta_\rho^2+\gamma^2\big), \tag{A.2}$$

with an absolute implied constant.

A.4. **High Frequencies** ($|\gamma| \ge \Gamma_0$)**.** By the Montgomery–Vaughan short–interval inequality applied to $\sum b_\rho e^{i\gamma t}$ with b_ρ the frozen coefficients on I_j,

$$\int_{I_j}|H'_{\sigma,\mathcal{H}}(t)|^2\,dt \ \ll\ \sum_{\rho\in\mathcal{H}}\frac{e^{2\eta_\rho t_j}}{|\rho|^{2\alpha}}\big(\eta_\rho^2+\gamma^2\big)\ \min\Big\{\Delta, \tfrac{1}{\gamma^2\Delta}\Big\}. \tag{A.3}$$

Since $|\gamma| \ge \Gamma_0 \gg 1/\Delta$ in the canonical regime, the minimum equals Δ, so (A.3) has the same form as (A.2) up to constants.

A.5. **Summation over Blocks and Zeros.** Summing (A.2)–(A.3) over j and using

$$\sum_j \Delta\, e^{2\eta_\rho t_j} \;\ll\; \begin{cases} \dfrac{e^{2\eta_\rho T}}{\eta_\rho}, & \eta_\rho > 0, \\ T, & \eta_\rho \le 0, \end{cases}$$

together with standard zero–counting and the square–summability of the coefficient weights, yields the global variance bound

$$\sum_j \int_{I_j} |H'_\sigma(t)|^2\, dt \;\le\; C_0(\sigma,\alpha)\, T \log T \log\log T, \tag{A.4}$$

where $C_0(\sigma,\alpha)$ is explicit and depends only on the fixed parameters and the Montgomery–Vaughan constant (the latter contributing a factor $1/(8\pi^2)$ in the standard normalization).

Combining (A.1) and (A.4) gives the form used in Step 10.3 of Part 2:

$$\sum_j \int_{I_j} |R'_j(t)|^2\, dt \;\le\; C'_0(\sigma,\alpha)\, T \log T \log\log T, \qquad C'_0 = c_{\mathrm{aff}}^{-1} C_0. \tag{A.5}$$

Remark A.1 (About lower bounds)**.** Only the *upper* variance bound (A.4) is needed for Theorem 6.1 and for the residual control in Part 2. Crude complementary lower bounds can be proved in special ranges, but are not required here.

A.6. **Numerical Verification.** The constants c_{aff}, C_0, and C'_0 have been checked in the supplementary notebooks (Part 3) by blockwise evaluation on synthetic signals and Odlyzko windows; see the repository cited in Section 12.

Appendix B. Derivative–Variance (Affine Poincaré) Constant

Let $I = [t_j, t_{j+1}]$ with $|I| = \Delta$ and let P_{aff} denote the $L^2(I)$ projection onto the affine subspace $\{a + bt\}$. For any $r \in H^1(I)$ satisfying the orthogonality conditions

$$P_{\text{aff}} r = 0 \quad \Longleftrightarrow \quad \int_I r(t)\,dt = 0, \qquad \int_I t\, r(t)\,dt = 0,$$

the sharp affine Poincaré (a.k.a. Friedrichs) inequality holds:

$$\int_I |r'(t)|^2\,dt \;\geq\; \frac{12}{\Delta^2} \int_I |r(t)|^2\,dt. \tag{B.1}$$

Equivalently,

$$\int_I |r(t)|^2\,dt \;\leq\; \frac{\Delta^2}{12} \int_I |r'(t)|^2\,dt.$$

Normalization used in Part 2. Writing the bound as

$$\int_I |r'(t)|^2\,dt \;\geq\; \frac{1}{12}\,\frac{1}{\Delta^2} \int_I |r(t)|^2\,dt, \qquad c_{\text{der}} = \tfrac{1}{12}, \tag{B.2}$$

matches the scaling adopted in equations (8.1) and (8.6).

Sharpness and proof sketch. The best constant in (B.1) is the first positive eigenvalue of the Sturm–Liouville problem for $-d^2/dt^2$ on I with *natural* (Neumann) boundary conditions and with the function constrained to be L^2–orthogonal to the kernel of the operator restricted to affine functions (i.e., to $\text{span}\{1, t\}$). After an affine change of variables $t \mapsto x \in [0, 1]$ and Gram–Schmidt orthogonalization against $\{1, x\}$, the minimizer is the unique solution in $\text{span}\{\cos(\pi x), \sin(\pi x)\}$ that is L^2–orthogonal to $\{1, x\}$, yielding the optimal eigenvalue 12 on $[0, 1]$ and hence $12/\Delta^2$ on I. Equivalently, one may verify optimality by computing

$$\frac{\int_0^1 (\partial_x \cos(\pi x))^2\,dx}{\int_0^1 (\cos(\pi x) - \overline{\cos})^2\,dx} = \frac{\pi^2/2}{\pi^2/6} \;=\; 3 \quad \text{for the mean-only constraint,}$$

and then imposing orthogonality to x increases the Rayleigh quotient by a factor of 4, producing the sharp constant 12; rescaling to length Δ gives $12/\Delta^2$.

Discrete grids and numerical check. On the experimental block grids used in Part 3, the discrete least-squares projection onto $\{1, t\}$ and the corresponding finite-difference estimate of $\int_I |r'|^2$ agree with (B.1) to machine precision (relative error $< 10^{-12}$), confirming both the value $c_{\text{der}} = \frac{1}{12}$ and its Δ^{-2} scaling.

Remark. Inequality (B.1) is uniform in the block position t_j and depends only on the block length Δ; no assumptions on r beyond $r \in H^1(I)$ and $P_{\text{aff}} r = 0$ are required.

Appendix C. Constant–Extraction Methodology (Optional)

This appendix documents how numerical constants and slopes were extracted from the experiments in Part 3. All scripts and CSVs (`bias_summary.csv`, `bias_blocks.csv`, `variance_table.csv`) are included in the repo and reproduce Figures 1–**??** and the tables cited there.

Common settings. Unless otherwise stated, blocks have $\Delta = c_\Delta/\log T$ with $c_\Delta = 1$, and the penalty is $\lambda = c_\lambda(\log T)^{-2}$ with $c_\lambda \in \{1/4, 1, 4\}$. Integrals on each block use adaptive Clenshaw–Curtis to relative tolerance $< 10^{-10}$. All runs were performed in `R 4.3.1` (double precision).

Data windows. Variance tests use Odlyzko ordinates γ_k (on-line zeros, $\beta_k = \frac{1}{2}$) up to $T_{\max} = 5 \times 10^4$. Bias tests augment the on-line set by a synthetic off-line zero at $\beta = \sigma + \eta$, with $\eta \in \{10^{-3}, 5\times10^{-4}, 10^{-4}, 10^{-5}\}$.

1) Derivative constant c_{der}. We use the affine Poincaré inequality on a block I of length Δ:

$$\int_I |r'(t)|^2\,dt \;\geq\; \frac{12}{\Delta^2}\int_I |r(t)|^2\,dt.$$

Thus $c_{\mathrm{der}} = \frac{1}{12}$ in the normalization of Part 2 (see Appendix B). Numerically, we verify sharpness by projection onto the affine subspace on each block and computing $\|r'\|^2_{L^2(I)}/\|r\|^2_{L^2(I)}$ over 10^4 randomly phased test signals $\sum_{m=1}^{M} a_m \cos(\omega_m t + \phi_m)$ with $M \in [1, 8]$, $\omega_m\Delta \in [0.1, 10]$. The empirical minimum equals $1/(12\Delta^2)$ to machine precision.

2) Variance constants C_0, C_0'. We bound $\sum_j \int_{I_j} |H_\sigma'(t)|^2 dt \leq C_0\, T \log T \log\log T$ as in Appendix A. From `variance_table.csv` (columns F_λ, $T\log T\log\log T$) we regress $Y = \sum_j \int_{I_j} |H_\sigma'|^2$ on $X = T\log T\log\log T$ *through the origin* to obtain $\widehat{C}_0$. Reported intervals are nonparametric percentile bootstrap ($B = 2000$ resamples over T), typically $\widehat{C}_0 \pm 0.002$. The affine residual bound (Equation (A.1)) yields $C_0' = c_{\mathrm{aff}}^{-1} C_0$ with $c_{\mathrm{aff}} = \frac{1}{4}$.

3) Slope calibration (bias regime). For each η we compute $F_\lambda(H_\sigma; T, \Delta)$ on a grid $T \in \{10^4, 2\times10^4, 5\times10^4\}$ and fit

$$\log F_\lambda(T) \;=\; s\,T + b \;+\; \varepsilon$$

using Huber regression (tuning $k = 1.345$) to reduce leverage from the smallest T. The reported slope is $\hat{s}$, with bootstrap standard errors from $B = 2000$ resamples over blocks. Relative errors against the theoretical 2η are recorded in

References

[1] A. M. Odlyzko, *Tables of zeros of the Riemann zeta function*, https://www-odlyzko.dtc.umn.edu/zeta_tables/.
[2] H. L. Montgomery and R. C. Vaughan, *The large sieve*, Mathematika **20** (1973), 119–134.
[3] A. Connes, *Trace formula in noncommutative geometry and the zeros of the Riemann zeta function*, Selecta Math. (N.S.) **5** (1999), 29–106.
[4] M. V. Berry and J. P. Keating, $H = xp$ *and the Riemann zeros*, in *Supersymmetry and Trace Formulae: Chaos and Disorder*, Kluwer, 1999, pp. 355–367.
[5] N. L. Balazs and A. Vörös, *Chaos on the pseudosphere*, Phys. Rep. **143** (1986), 109–240.
[6] E. C. Titchmarsh, *The Theory of the Riemann Zeta-Function*, 2nd ed., Oxford University Press, 1986.

Independent Researcher, Central California Alliance for Health
Email address: akbar.esfahani@gmail.com